JOURNAL OF APPLIED ELECTROCHEMISTRY 23 (1993) 1263–1267

Measurement of anode potentials at high current densities by the current interruption method for metals used in aviation technology

J. HÍVEŠ

Slovak Technical University, Department of Inorganic Technology, Radlinského 9, 812 37 Bratislava, Slovakia

I. ROUŠAR

Prague Institute of Chemical Technology, Department of Inorganic Technology, Technická 5, 166 28 Prague, Czech Republic

Received 16 October 1992; revised 5 April 1993

An electochemical flow-through cell and a current-interruption technique were used to investigate the potential of anodes made from mild steel, nickel, and four Ni–Cr–Fe alloys at high current densities (from 1 up to 100 A cm^{-2}) in NaCl solutions for a Reynolds number of 7370. A plot of the anode potential against logarithm of current density yielded a Tafel line over a broad range of current densities. The plateau on the anode potential against current density curve was attributed to salt film formation. This explanation was confirmed by visual observation of the anode surface.

1. Introduction

Values of anodic potentials at high current densities for materials used in aviation technology are necessary for the calculation of local current densities during electrochemical machining (ECM). The *IR*-free anodic potentials (e.g. potentials corrected for voltage drop in the electrolyte) at high current densities for mild steel and nickel electrodes in sodium chloride solutions have been studied by a number of authors [1–7], but the slopes of the polarization curves were very varied over a very broad range, see Fig. 1. For instance the *IR*-free anodic potential of mild steel varied from 0 up to 9 V vs NHE at a current density of 100 A cm^{-2}. This is due to different experimental methods used for the estimation of the anodic potential, the type of the electrochemical cell and mainly by the uncertainty in the *IR* subtraction. A constant current interrupter technique was usually employed in the experimental determination of anode potentials during high-rate anodic dissolution of metals [1, 2, 5–9]. The anodic polarization curves for mild steel in NaCl solutions were summarized by Davydov [10] and, with additional data, are schematically shown in Fig. 1. The polarization curves were obtained by the current interruption method in nonstirred solution [2, 7] by the direct method in a flow-through channel cell ($u = 6$ and 1 m s^{-1}, [3, 4]), by the current interruption method in a flow-through channel cell ($u = 20$ m s^{-1}, [5]), and by the current interruption method in a quiet solution [1, 6]. The kinetics and the stoichiometry of the anodic dissolution at high current density of multicomponent alloys based on iron and nickel are not well known, but the anodic behaviour of iron and nickel has been studied by a number of authors [11–17]. For iron dissolution in chloride solutions, the stoichiometry and the resulting surface finish depend strongly on the mass transport conditions at the electrode. Below the limiting (critical) current density corresponding to salt film precipitation on the anode surface, the dissolution of iron yields divalent ions. Trivalent ions were produced and surface brightening of the anode was observed when the limiting current density was reached [15].

The purpose of the present study was to evaluate the anodic potentials of mild steel, nickel, and Ni–Fe–Cr alloys in NaCl solution at high anodic current densities, which are necessary for the calculation of the local current densities during ECM. The anodic polarization curves of mild steel and nickel were used as references.

2. Experimental details

In the present study a flow-through cell was used. The construction of the cell and experimental setup was similar to the arrangement used by Landolt [15]. The electrolyte was continuously circulated by means of a piston pump and contained in a 5 dm^3 PVC reservoir. The body of the electrochemical cell consisted of two rectangular blocks made of polyacrylic glass. Into one of these blocks a rectangular electrolyte flow channel 0.4 mm deep, 3 mm wide and 73 mm long was grooved. A thick platinum wire, diameter equal to 1.13 mm, (1 mm^2 cross section) was used as a fixed cathode; this was positioned opposite an anode wire of the same free electrode area. The distance between

0021-891X

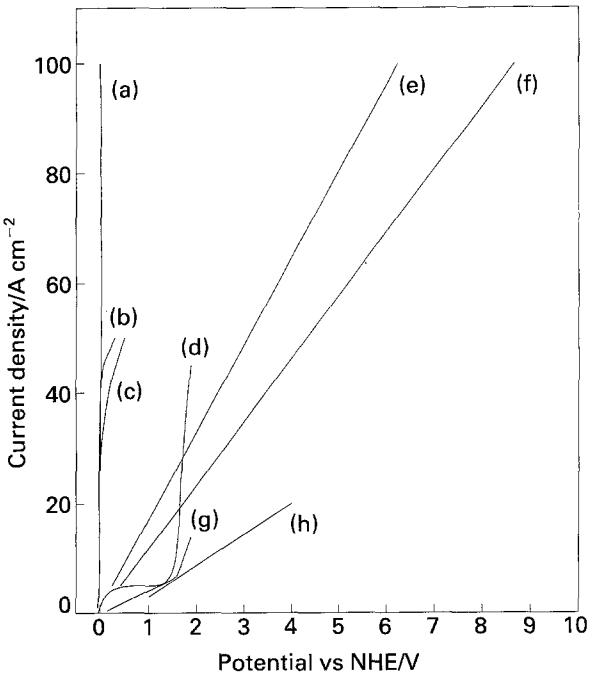

Fig. 1. Anodic polarization curves for mild steel electrodes in NaCl solutions according to references (a) 20% [7], (b) 20% [2], (c) 15% [4], (d) 15% [3], (e) 20% [5], (f) 10% [5], (g) 18% [6], (h) 20% [1], composition is in wt %.

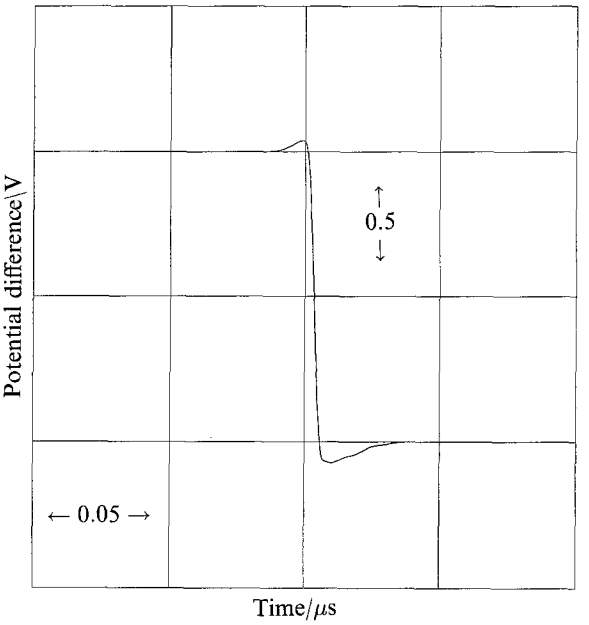

Fig. 2. Transient curve $U = f(\tau)$ of the interrupter; horizontal resolutions 0.05 μs div^{-1}., vertical resolution 0.5 V div^{-1}, $R = 1.00\,\Omega$, $I = 1$ A, measured by analogue oscilloscope (Tektronix 2235A).

the electrodes was 0.4 mm (the same as the channel depth) and was fixed by a micrometric screw. The leading edge of the working electrode was positioned 61 mm downstream from the channel inlet. This corresponds to 86 hydraulic diameters (defined by 4× cross section/circumference), enough to guarantee fully developed velocity profiles at the electrodes under both laminar and turbulent flow conditions. The cell assembly was held together with ten brass screws. A small capillary hole (0.8 mm) was drilled upstream of the anode (at a 0.3 mm distance from the anode) providing connection (Luggin capillary) to the Ag/AgCl reference electrode. A 8 mm thick and 15 mm long silver screw with a cavity formed the reference electrode. The inner surface of the cavity was electrochemically covered with AgCl and the cavity was filled with a 20% NaCl solution. To decrease the ohmic drop in the connecting capillary, a silver wire covered with AgCl was positioned in it and connected to the silver screw. This arrangement provided a low-impedance circuit, well suited for fast transient studies. A 1250 Solartron frequency analyser and 1186 electrochemical interface were used for the measurement of the cell impedance. The a.c. amplitude was 5 mV, the frequency was in the 0.1–64 kHz range, the anode d.c. applied current density was 0.01 A cm^{-2}, $Re = 10\,000$. For this purpose a solution of 0.03 M $K_3Fe(CN)_6$, 0.3 M $K_4Fe(CN)_6$, and 0.5 M KOH was prepared from reagent grade chemicals and distilled water. The solution was deaerated by bubbling nitrogen. Experiments were carried out at 25 ± 1° C, nickel electrodes (cathode, anode and reference electrode) were used. The measured impedance diagram was represented by a semicircle, see [21]. The current interruption method was used to measure the *IR*-free anodic potentials. A constant current was applied to the cell by a potentiostat (Weking 75LB). The current was measured by using a precision 5.1 Ω resistance. The anode potential vs Ag/AgCl reference electrode and the voltage drop on the 5.1 Ω resistor were displayed and stored in digital form every 50 ns by a two-channel fast transient recorder (DL-912, 8 bits, 2 memories, each 4 Kbyte data capacity). The current was interrupted with a FET transistor (transition time less than 10 ns). The interrupter was tested using an analogue oscilloscope (Tektronix 2235A); the applied current was 1 A on a 1.0 Ω resistor. A transient curve $U = f(\tau)$ is shown in Fig. 2. Before the measurement, a constant charge of 20 C cm^{-2} was passed through the cell in the galvanostatic mode and then the current was interrupted. This charge assured that a steady state was reached in the system. Before the experiment, the anode surface was polished with wet 600 grit grinding paper, rinsed with distilled water, and immediately transferred to the flow cell. A 20% NaCl solution was prepared from reagent grade NaCl (Lachema, Brno) and distilled water. A fresh electrolyte was prepared for each anode material. All experiments were conducted at 25 ± 1° C. The potential of the Ag/AgCl reference electrode was checked against SCE before and after each run. Differences in the reference electrode potential during the experiments were less than ±2 mV.

3. Results and discussion

After a charge of 20 C cm^{-2} had passed, the current was interrupted and a transient curve of the anode potential against time was recorded. Figure 3 shows the potentials of the mild steel anode before and after the current interruption at a current density of 99 A cm^{-2}. The accuracy of the measured anodic

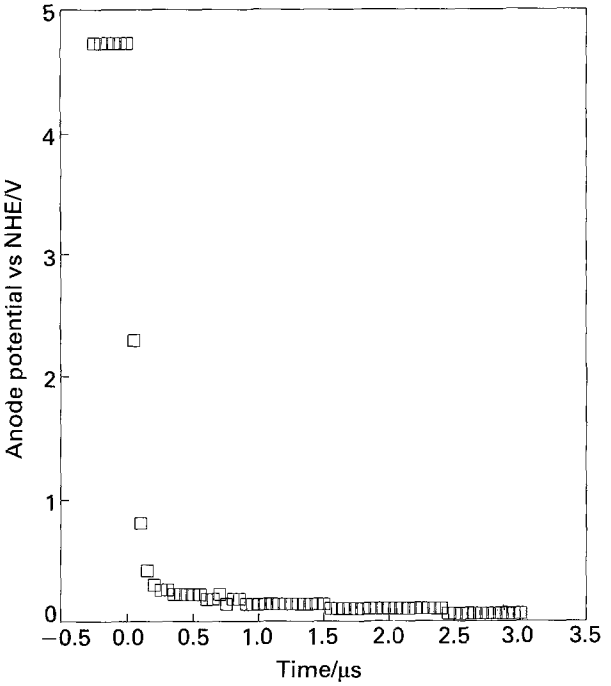

Fig. 3. Potential decay of a mild steel anode in 20% NaCl at 99 A cm^{-2}. The linear flow velocity of the electrolyte was 14 m s^{-1}, $Re = 7370$.

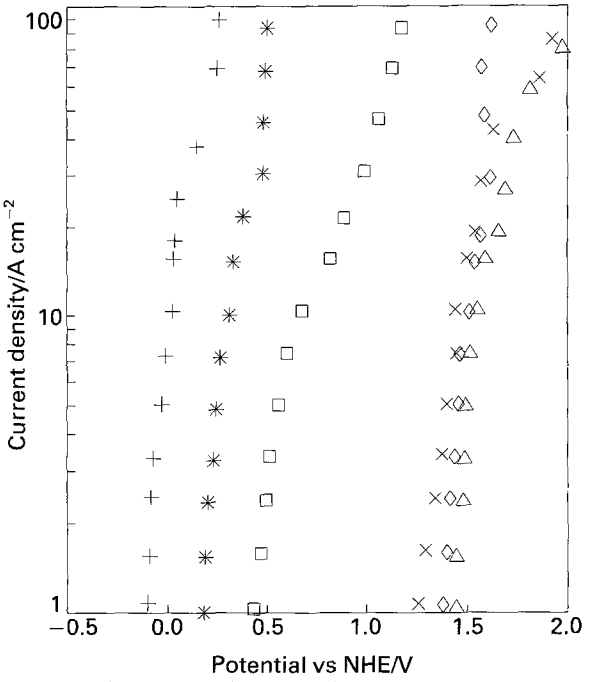

Fig. 4. Plot of *IR*-free anodic potential vs. current density in 20% NaCl. The linear flow velocity of the electrolyte was 14 m s^{-1}, $Re = 7370$, (+) mild steel, (*) AK1, (□) nickel, (x) LVN10, (◇) EI437, (△) EI617.

potentials at high current densities is mainly limited by two factors: the estimation of the *IR* drop in the solution and the estimation of the rate of double layer discharge. The measured voltage before interruption is a sum of *IR* drop and the anodic potential. The value of $E_A(\tau = 0)$ was found from the double layer discharge estimated by Equation 1 on the assumption of constant double layer capacity and the validity of Tafel kinetics for the anodic reaction [20]:

$$E_A(\tau) = E_A(\tau = 0) - b \ln\left(1 + \frac{j\tau}{bC}\right) \qquad (1)$$

where

$E_A(\tau)$	formal anodic potential (V)
$E_A(\tau = 0)$	formal *IR*-free anodic potential (V)
b	Tafel slope (V); from $\eta = a + b \ln(j)$
j	applied anodic current density before current interruption (A cm^{-2})
τ	time after interruption (s)
C	double layer capacity (F cm^{-2})

Owing to limitations in the frequency response of the DL-912 amplifiers (6 MHz upper limit), the value of $E_A(\tau = 0)$ cannot be determined exactly. From the measured $E_A(\tau)$ values it was inferred that the error in $E_A(\tau)$ values, measured after interruption at 50, 100 and 150 ns, was due to the limited frequency response of the amplifiers. Therefore, Equation 1 was used as a base for a non-linear regression fit of the anodic potential transient in the range 200–3000 ns, which yielded the *IR* drop, the Tafel slope and the double layer capacity (Table 1). Equation 1 is not valid in the region of the limiting (critical) current density. The use of Equation 1 close to the critical current density causes problems, e.g. unrealistic values of b and other parameters in this region are calculated. The confidence interval for b is large owing to the contribution of the values calculated in the region near the critical current density. Figure 4 shows the *IR*-free anode potential against current density plot on a semilogarithmic scale for all metal materials used at a linear flow velocity of 14 m s^{-1} ($Re = 7370$). Apparently, the *IR*-free anode potential is linearly related to the logarithm of the current density, in good agreement with the assumption of Tafel behaviour of the anode materials, whose composition is given in Table 2.

Table 1. Average values of the Tafel slope and double layer capacity for the anode materials used

Anode material	*Tafel slope* b/mV	*d.l. capacity* C/μF cm^{-2}
Mild Steel	20 ± 10	46 ± 16
AK1	104 ± 17	12 ± 2
Nickel	174 ± 16	2 ± 1
LVN10	43 ± 41	17 ± 8
EI437	42 ± 23	17 ± 5
EI617	146 ± 63	37 ± 2

The polarization curve of mild steel exhibits some distortion at a current density of 50 A cm^{-2} (critical current density) and the anodic potential is shifted to higher values, as expected from polarization curves measured at the lower current density. This distortion and the change of the slope of the polarization curve shown in Fig. 4 may be caused by an anodic salt film. Visual observation of the anode surface after the experiments clearly showed that the surface of the anode obtained below the critical current density was porous and black. Above the critical current density, the surface of the electrode became bright and glossy. This observation is in good agreement with

Table 2. Composition of the anode materials according to [15]

	AK1	*EI617*	*EI437*	*LVN10*	*Mild Steel*	*Nickel*
Ni	1.65	74	74	74	–	99.9
Cr	11.25	14.5	20.5	12.5	–	–
Fe	82	5	1.0	0.5	98.64	0.1*
Al	–	2	0.8	6	–	–
Mo	0.42	3	–	4.5	–	–
Ti	–	1.05	2.7	0.7	–	–
W	1.8	–	–	–	–	–
V	0.24	1.3	–	–	–	–
C	0.13	0.06	–	0.03	0.1	–
B	–	0.2	0.01	0.01	–	–
Si	0.6	0.6	–	0.5	–	–
Cu	0.3	0.07	0.07	0.3	–	–
Mn	0.6	0.5	0.4	0.2	0.9	–
S	0.025	0.01	0.07	0.015	0.18	–
P	0.03	0.015	0.016	0.015	0.18	–
Ce	–	0.2	0.01	–	–	–
Pb	–	–	0.01	–	–	–
Nb + Ta	–	–	–	2.0	–	–
Zr	–	–	–	0.10	–	–
Sn + Sb	–	–	1.0	–	–	–

*Fe + Co

other authors [13–15]. A similar behaviour was observed with the material AK1. The transition region in the appearance of the anode surface from etching to brightening was broader for pure nickel and corresponded to a change in the double layer capacity with current density for the nickel electrode. From Fig. 5 a considerable change in the double layer capacitance is visible above 15 A cm^{-2}. From Fig. 4 it follows that the kinetic parameters are changing in this current density range and this influences the apparent capacity. Nevertheless, because at each point all parameters (*IR* drop, *b*, *C*) are evaluated from the potential-time transient curve, the apparent capacity represents local value for a given current density. There is no averaging over all current densities. This is the reason why the value of the apparent capacity primarily represents the change in surface properties for a given electrochemical reaction. The polarization curve for LVN10 also exhibits a sudden change in anodic potential slope at a current density of 50 A cm^{-2}. The alloy EI617 showed similar behaviour, but the critical current density was 20–40 A cm^{-2}. The polarization curve for EI437 exhibits a negative change in the anodic potential slope above 40 A cm^{-2}. This unrealistic part of the polarization curve is probably due to errors in the *IR* drop estimation. The error in conversion by the 8 bit A/D converter is 20 mV for the 5 V scale and this may cause the observed error in anodic slope. The expected linear behaviour of the current density against *IR* potential drop on log-log coordinates can be seen from Fig. 6. On the basis of regression analysis using the equation

$$\log j = k_1 + k_2 \log(IR) \qquad (2)$$

we obtained $k_1 = -0.34 \pm 0.04$ and $k_2 = 0.98 \pm 0.03$ for a 95% confidence interval. This result means that the estimated R value is independent of the applied current density.

4. Conclusion

The interruption technique was used for the estimation of the anodic potential of mild steel, nickel and four metal alloys at current densities up to 100 A cm^{-2} in a flow channel cell at a Reynolds number of 7370. The use of Equation 1 for the evaluation of transient values of $E_A(\tau)$ enabled the

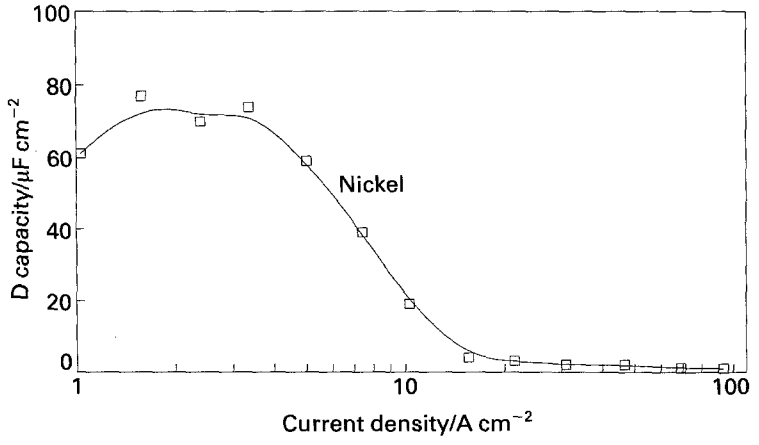

Fig. 5. Plot of double layer capacity against current density for a nickel anode in 20% NaCl. The double layer capacity was evaluated from the transition curves by using Equation 1. The linear flow velocity of the electrolyte was 14 m s^{-1}, Re = 7370.

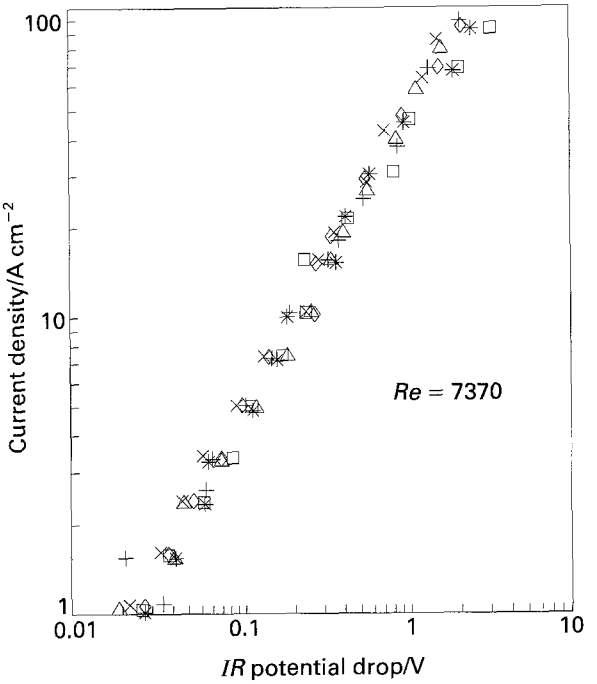

Fig. 6. Plot of *IR* potential drop vs current density in 20% NaCl. The linear flow velocity of the electrolyte was 14 m s^{-1}, $Re = 7370$, (+) mild steel, (*) AK1, (□) nickel, (x) LVN10, (◇) EI437, (△) EI617.

estimation of Tafel slopes for all these materials as functions of current density. The Tafel slopes, $dE/d\log j$, are in the range from 20 to 174 mV. On the *IR*-free polarization curves a plateau was observed, and the corresponding current density was denoted as critical current density due to the formation of a salt film on the anode surface; this was supported by visual observation. The measured polarization curves can be used to calculate the local current densities during electrochemical machining of the studied materials [19].

References

[1] J. N. Petrov, *Elektronnaya obrabotka materialov* No. 26 (1969) 30.
[2] A. D. Davydov and V. D. Kascheev, *Fizika i khimiya obrabotki mat.* No. 5 (1968) 40.
[3] A. D. Davydov, V. D. Kascheev, R. A. Mirozev, *ibid.* No. 10 (1973) 32.
[4] A. D. Davydov and V. D. Kascheev, *Elektrokhimiya* **10** (1974) 154.
[5] K. W. Mao, *J. Electrochem. Soc.* **120** (1973) 1056.
[6] A. V. Vvedenskii, *Elektronnaya obrabotka materialov* no. 55 (1974) 79.
[7] K. Chikamori, H. Yamamoto, S. Ito, Proceedings of the International Conference on Production Engineering, The Japan Soc. of Prec. Engg., Tokyo (1974) p.68.
[8] D. Landolt, R. H. Müller and C. W. Tobias, *J. Electrochem. Soc.* **118** (1971) 40.
[9] D. Landolt, *ibid.* **119** (1972) 708.
[10] A. D. Davydov, *Elektronnaya obrabotka materialov* no. 5 (1975) 19.
[11] D. T. Chin and A. J. Wallace, *J. Electrochem. Soc.* **120** (1973) 1487.
[12] M. L. McMillan and M. A. LaBoda, *J. Electrochem. Techn.* **5** (1967) 346.
[13] D. T. Chin, *J. Electrochem. Soc.* **118** (1971) 174.
[14] H. C. Kuo and D. Landolt, *Electrochim. Acta* **20** (1975) 393.
[15] M. Datta and D. Landolt, *ibid.* **25** (1980) 1255.
[16] A. D. Davydov, B. N. Kabanov, V. D. Kascheev, *Fizika i khimiya obr. mater.* no. 4 (1972) 139.
[17] A. D. Davydov, E. N. Kirjak, V. D. Kascheev, *Elektrokhimiya* **14** (1980) 1420.
[18] P. Novák, I. Roušar, R. Štefec, *Mater. Chem. & Phys.* **10** (1984) 155.
[19] J. Híveš and I. Roušar, to be published.
[20] A. N. Frumkin, *Acta Physicochimica, USSR* **18** (1943) 23.
[21] J. Dvořák and J. Koryta, Elektrochemie, Academia, Prague (1983) p.293.